UCRL - 76888
PREPRINT

LAWRENCE LIVERMORE LABORATORY
University of California/Livermore, California

THEORY OF HIGH DENSITY LASER FUSION

G. B. Zimmerman and J. H. Nuckolls

May 27, 1975

This Paper Was Prepared for Presentation at
The Canadian Association of Physicists, Plasma Summer School on Fusion
Banff, Alberta, June, 1975

THEORY OF HIGH DENSITY LASER FUSION*

G. B. Zimmerman and J. H. Nuckolls
University of California, Lawrence Livermore Laboratory, Livermore, CA.
United States of America

I. Introduction

Among the proposals for generating electrical power from inertially-confined, laser-initiated thermonuclear reactions, those involving high fuel compressions[1,2,3] require the smallest laser energies. This can be seen from the following simple model: In order to achieve efficient thermonuclear burning a given plasma temperature ($\sim$10 keV) must be reached. The laser energy required then will be proportional to the target mass ($E_L \alpha M$). As with magnetic CTR the thermonuclear burn efficiency is proportional to $\rho\tau$ where ρ is the matter density and τ the confinement time, but for inertially confined plasmas $\tau \alpha R$, the fuel radius. For a given burn efficiency (fixed ρR) the required laser energy then becomes

$$E_L \alpha M \alpha \rho^{-2}(\rho R)^3 \alpha \rho^{-2}$$

*Work performed under the auspices of the U. S. Energy, Research and Development Administration.

The laser power, also a practical constraint, is similarly shown to be

$$P_L \alpha E_L/\tau \alpha M/R \alpha \rho^{-1} (\rho R)^2 \alpha \rho^{-1}.$$

Thus both the laser energy and power are reduced as the matter density is increased.

Many important physical processes that have been ignored in this model, will be discussed later. These determine the optimal degree of compression and also place several other constraints on the design of both target and laser. Sophisticated computer simulation techniques have been used to analyze the relevant plasma, transport, hydrodynamic and atomic processes; but numerous theoretical problems remain unsolved. Experimental results, although encouraging, are far from confirming the feasibility of laser fusion CTR.

A basic laser fusion scheme is presented in Section II. In Section III we discuss some of its subtleties and consider the theoretical difficulties which now appear to be the major obstacles. Interpretations of some recent laser compression experiments are given in Section IV.

II. An Idealized Laser-Fusion Model

A. Compression

At constant mass, compression causes the ρR of the plasma to increase. This improves burn efficiency because it increases the reaction rate faster than the confinement time decreases. In addition, the 3.5 MeV alpha particles produced from DT reactions will deposit their energy within a range ~ 0.3 g/cm^2 in 10 keV matter. Thus, for $\rho R > 0.3$ g/cm^2 only the innermost 0.3 g/cm^2 need be heated hydrodynamically to the 10 keV ignition temperature. The alpha energy deposited initiates a thermonuclear burn front which ignites the remainder of the compressed fuel, thus saving ignition energy that would otherwise have to be supplied by the laser.

The advantages of compression are limited by depletion of the DT fuel and by the PdV work required to compress even cold matter to super-high densities. The latter limitation is imposed by Fermi-degenerate electron pressure

$$P_{F-D}(\text{atm}) \approx 10^{12} \left(n_e / 5 \times 10^{26}\right)^{5/3}$$

where n_e is the electron number density (cm^{-3}). Computer simulations have found that 10^4 fold compression ($\rho \sim 2 \times 10^3$ g/cc) of ~ 20 μg of DT

($\Rightarrow \rho R \approx 2$) are near optimal conditions for a 5×10^4 J laser. Under these conditions the Fermi-degenerate compressional energy

$$E_c \approx 10^3 \text{ J } (\rho / 2 \times 10^3)^{2/3} \text{ (M/20 μg)}$$

is comparable to the 10 keV ignition energy of the central 2 μg of fuel. The total compressional and ignition energy ($\sim 2 \times 10^3$ J) is only ~5% of the laser energy deposited due to inefficiencies of the implosion scheme.

B. Thermonuclear Burn

The thermonuclear burn efficiency ϕ, adjusted to account for depletion, can be written[4]

$$\phi / (1-\phi) \approx \rho R \langle \sigma v \rangle / 8 c_s m_i \qquad (1)$$

where $\langle \sigma v \rangle$ is the Maxwell-averaged DT reaction rate, $c_s = (10 \text{ kT}/3m_i)$ is the sound speed and m_i is the average ion mass. A plot of $\phi/(1-\phi)$ versus temperature T maximizes between 20 and 50 keV and is relatively flat in this range. Evaluating Eq. (1) here we obtain

$$\phi \approx \frac{\rho R}{\rho R + 6} \quad .$$

Thus, at $\rho R \approx 2$, approximately 25% of the 20 μg of fuel burns giving 3×10^6 J of thermonuclear energy. This is adequate to run a power plant with a 40% thermal-to-electrical efficiency and a 10% efficient 5×10^4 J laser.

Theoretical gain curves (thermonuclear energy/laser energy) for different laser energies as a function of compression are given in Figure 1. Each point represents an optimization over other parameters (such as fuel mass and laser pulse shape); and the curves have been normalized to computer simulations. The curves show a maximum because of the inefficiency of thermonuclear burn at low ρR and the cost of compressing even degenerate matter to very high density. For numerous reasons, including the symmetry and stability of the implosion scheme, these results are probably optimistic.

C. Implosion

The minimum pressure of DT at density 2×10^3 is 10^{12} atmospheres. Such pressures can be generated by a spherical implosion system which focuses laser energy densities in both space and time.

Laser light propagates through a low density atmosphere surrounding the fuel pellet. When it nears the critical density, where the plasma and light frequencies are equal, it is absorbed by inverse bremsstrahlung and collective plasma processes. The critical density is given by

$$\rho_c = 4 \times 10^{-3} \, (\omega/\omega_{Nd})^2 \qquad (2)$$

where ω/ω_{Nd} is the ratio of light frequency to that of a neodymium laser. A lower limit on the electron temperature produced by this absorption can be obtained by equating the laser intensity to the free-streaming electron energy flux

$$I = n_c v_e \, k \, T_e$$

where $n_c = 10^{21} \, (\omega/\omega_{ND})^2$ is the critical electron density, $v_e = (k \, T_e/m_e)^{1/2}$ is the electron thermal velocity and T_e is the electron temperature. For neodymium light and an intensity of 10^{16} W/cm^2 we find $T_e \sim 10$ keV and a pressure at critical density of $P_c \sim 2 \times 10^7$ atmospheres.

If the atmosphere is nearly isothermal, then electron transport will create higher pressures in the higher density region near the pellet (ablation) surface. Here the oppositely directed temperature and density gradients form a pressure peak that explodes the pellet surface layers. This ablation pressure may be estimated by equating the rate of hydrodynamic work done at the ablation surface to the power transported from the critical surface by electron transport

$$P_A \, A_A \, c_s = P_c \, A_c \, v_e$$

$$P_A = P_c \, (A_c/A_A) \, (v_e/c_s)$$

$$\approx P_c \, (A_c/A_A) \, (m_i/m_e)^{1/2}$$

where $A_c/A_A \sim 10$ is the ratio of critical to ablation surface areas. The ablation pressure then is 10^{10} atmospheres.

The final factor of 10^2 in pressure is achieved by applying the ablation pressure over a volume much larger than that of the final compressed fuel. This PdV work is used to create inward directed kinetic energy which is ultimately re-converted to internal energy as the matter collapses upon itself. This pressure amplification through implosion is capable of generating the necessary 10^{12} atmospheres, but it must be done very carefully in order to have all the kinetic energy re-converted to internal at nearly the same time. Care also must be taken to generate as little entropy as possible (to keep the matter Fermi-degenerate) and to heat only the central region of the compressed fuel to ignition temperatures.

D. Pulse Shape

Computer simulations, and subsequently, an analytic theory[5], have shown that these implosion characteristics can be generated by optimally tailoring the laser power in time. The laser pulse for a 50 μg liquid DT drop (Figure 2) starts at a power level just sufficient to generate a 1 cm/μs shock (approximately the sound speed in liquid DT). The power is subsequently raised so that the hydrodynamic flow characteristics in the pellet intersect only near the center where shock heating is desired to facilitate ignition. The total laser pulse length is approximately the transit time of the initial shock.

The final laser power, 5×10^{14} W, would be difficult and costly to produce, and may not even be useful because of electron decoupling effects to be discussed later. The peak laser power may be reduced by using thin, hollow shells of frozen DT as targets. In this way the ablation pressure acts over an even larger volume; and larger pressure amplification can be achieved by implosion. The aspect ratio of the shell $R/\Delta R$, however, is probably restricted to values $\lesssim 5$.[6] We will see that larger values lead to shell breakup caused by fluid (Rayleigh-Taylor) instabilities.

III. Theoretical Problem Areas

In the previous section we have discussed an idealized laser fusion scheme. We have assumed that a substantial fraction of the incident laser light is absorbed, that the electrons heated at critical density can collisionally couple their energy to the more numerous colder electrons at the ablation surface, and that the implosion process is not substantially altered by non-uniform laser illumination or the growth of fluid instabilities. These assumptions will now be addressed.

A. Absorption - Reflection

At low electron temperatures laser light is effectively absorbed by inverse bremsstrahlung. The reciprocal absorption length for this collisional process is[7]

$$\kappa_{IB}\ (cm^{-1}) = 30\ Z\ (\rho/\rho_c)^2\ (1 - \rho/\rho_c)^{-1/2}\ (\omega/\omega_{Nd})^2\ T_e^{-3/2} \qquad (3)$$

where Z is the effective charge, ρ/ρ_c the ratio of density to critical density, and T_e the electron temperature in keV. For high temperatures ($T_e \geq$ 10 keV) or long wavelengths ($\omega/\omega_{pd} < 1$) inverse bremsstrahlung is unable to absorb a large fraction of the laser energy.

Additional processes, notably parametric decay instabilities and resonance absorption, have been studied with two-dimensional relativistic computer simulations.[8] Figure 3 gives the fractional absorption as a function of incident angle (measured from the normal) due to these processes. In these calculations a self-consistent density profile (determined by balancing electromagnetic, matter, and ram pressures) is used. At normal incidence the light reaches nearly to the critical density and absorption is dominated by parametric decay instabilities. Resonance absorption peaks at angles $\sim$15° from normal because it requires a component of the electric field parallel to the density gradient. These calculations assumed that the laser light was polarized in the incident plane. The fractional absorption due to resonance absorption will be decreased by a factor of two for random polarizations. Thus, $\sim$30% absorption might be expected, but this could be much larger if the critical surface is broken up by fluid-like instabilities.[9] Experimental measurements of absorption lie between 20 and 80% with at least part of the variation being due to different pulse shapes that produce different initial density profiles.

Other plasma instabilities (Brillouin and Raman) will tend to reflect rather than absorb the laser light. Computer simulations have shown that this reflection can be substantial[10,11], but also that these instabilities may effectively turn themselves off by steepening the density gradient[12]. The time-dependent reflectivity measured at the University of Rochester[13] may be experimental verification of density gradient steepening. More theoretical and experimental work is needed before these abosrption and reflection processes are adequately understood.

B. Heated Electron Distribution

The Coulomb cross-section is a strongly decreasing function of particle energy. Inverse bremsstrahlung, a collisional process, therefore heats predominately low-energy electrons and produces an essentially thermal electron distribution. Collisionless processes, however, tend to heat those electrons whose velocities are high enough to allow phase matching to plasma waves. Plasma simulation calculations[12] show that both resonance absorption (Figure 4a) and parametric instabilities (Figure 4b) produce electron distributions with high energy non-Maxwellian tails. The heated electron energy is typically less for resonance than for parametric instability absorption.

Such high energy electrons have been observed in microwave experiments[14]. X-ray spectra from laser irradiation experiments often show high energy tails that may indicate the generation of non-Maxwellian electron distributions. These x-ray spectra, however, might also be produced by Maxwellian electrons

if their transport is substantially reduced by the presence of ion fluctuations or magnetic fields. If such high energy electrons are produced, they may preheat the fuel, making it difficult to compress.

C. Electron Transport

Energy is transported from the absorption (critical) surface to the pellet (ablation) surface by electron conduction. If this heat flow is severely restricted, then the desired ablation pressures cannot be generated. Classically, the energy flow is

$$\underset{\sim}{Q} = -\kappa_e \underset{\sim}{\nabla} T_e$$

where $\kappa_e = \frac{3}{2} n_e k \lambda_e v_e / 3$

is the electron conductivity[15] and $\lambda_e \propto T_e^2$ is the collisionally-determined electron mean-free-path. This heat flow is clearly limited by the maximum flux that can be carried by free-streaming electrons ($Q \sim n_e v_e k T_e$), but may be further restricted by charge fluctuations or magnetic fields.

If the electron-ion temperature ratio is large ($T_e/T_i \geq 3$) and the electron drift velocity $v_d = Q/(n_e k T_e)$ exceeds the ion acoustic velocity ($v_A \approx c_s$), then an electron-ion two-stream instability will develop[16]. If this instability can grow to the "wild turbulence" limit (which may require unrealistically large ion fluctuations), then the electron heat flow may be

reduced to $Q \sim n_e c_s k T_e$. Such a restricted heat flow has been found to be consistent with several experimental observations, including x-ray spectra and ion flux data[17].

Multi-megagauss magnetic fields can be generated in a laser-heated plasma by non-parallel electron pressure and density gradients[18]

$$\dot{\underset{\sim}{B}} = \underset{\sim}{\nabla} \times \left(\frac{c}{e n_e} \underset{\sim}{\nabla} P_e \right) \qquad (4)$$

or from the momentum imparted to electrons by non-normally incident laser light[19]. Fields of this size have been measured experimentally in laser-produced plasmas by magnetic probe[20] and Faraday rotation[21] methods. Classical electron heat flow across such magnetic fields would reduce the usual electron conductivity to $\kappa_e' = \kappa_e (\omega_e \tau_e)^{-2}$ where $\omega_e = eB/m_e c$ is the electron gyro-frequency and $\tau_e = \lambda_e / v_e$ is the collision time[22]. This reduction in electron conductivity can be expressed as

$$\frac{\kappa_e'}{\kappa_e} = .04 \left(\frac{B}{10^6 G} \right)^{-2} \left(\frac{n}{10^{21}} \right)^{2} \left(\frac{T}{1\ keV} \right)^{-3} \qquad (5)$$

showing its importance at the low densities and high temperatures characteristic of laser-heated plasmas. Under nominal conditions the magnetic energy density $B^2/8\pi$ is $\lesssim 1\%$ of the plasma pressure. Thus the magnetohydrodynamic $\underset{\sim}{j} \times \underset{\sim}{B}$ force will be small. Based on experience with magnetically confined plasmas, it is difficult to believe that such a small field can contain electron energy to

the degree that Eq. (5) predicts. In one model[23], plasma turbulence develops to a level such that electrons effectively scatter every gyro-period. This Bohm diffusion[24] reduces the electron conductivity to $\kappa_e'' \approx \kappa_e(\omega_e \tau_e)^{-1} \approx (\kappa_e \kappa_e')^{1/2}$. The type of electron transport (either classical or Bohm) across magnetic fields in laser-produced plasmas has not been determined theoretically or experimentally. The distinction may be important to the success of laser fusion, expecially for CO_2 laser light which is absorbed at low density ($n_c = 10^{19}$).

D. Decoupling - Preheat

Good electron conductivity is necessary, but is not sufficient to create high ablation pressures at the pellet surface. We must also require that the transported energy be coupled to the high density matter near the ablating surface. In the absence of energy coupling, electrons heated by laser light absorption will stream throughout the pellet atmosphere and quickly establish a uniform number and energy density. The pressure then will be uniform, rather than proportional to matter density.

This electron decoupling[25] can occur if the heated electron mean-free-path is larger than the radius of the absorption surface. If the electrons are unable to lose their energy while crossing the pellet atmosphere, they will return to the absorption region and be heated to higher energies. Since the Coulomb cross-section falls off with increasing electron energy, this can

lead to a runaway condition. The decoupling problem can be minimized by using short-wavelength lasers ($\lesssim 1\mu m$) which heat more electrons to lower energy, and by using hollow targets that require lower laser power.

Another problem associated with high energy electrons is that they may burrow deep into the imploding fuel. Even a small amount of this preheat energy can raise the fuel entropy and make it difficult to compress. The severity of the preheat and decoupling problems, as well as methods of minimizing their effects, have been extensively studied by Lindl[26].

E. Symmetry - Stability

The discussions to this point have considered only one-dimensional spherical implosions. Non-uniform laser irradiation and pellet fabrication imperfections necessitate two and three-dimensional considerations. Compression of a sphere by 10^4-fold requires the radius to decrease by a factor of 20. If the compressed core is to be spherical to within a factor of 2, then the ablation pressure must be uniform to $\sim 2\%$. A multiple (~ 10) beam laser irradiation system is expected to achieve illumination uniformity of $\sim 10\%$. The additional smoothing is obtained by electron conduction in the pellet atmosphere; but this is effective only if the absorption radius is kept a factor of two larger than the ablation radius. Symmetry difficulties are less severe for long wavelength (CO_2) laser light.

The effects of fluid instabilities on laser-fusion pellets have been studied by linear perturbation techniques[27, 28], and by direct simulation of the two-dimensional hydrodynamic flow[6]. The two methods are in general agreement. Fluid instabilities are most severe for hollow-shell targets and for perturbation wavelengths comparable to the shell thickness ($\lambda \sim \Delta R$). The classical Taylor instability growth rate is[29]

$$\gamma = \sqrt{a\,k} \tag{6}$$

where a is the acceleration and $k = 2\pi / \lambda$. The total number of perturbation e-foldings is $N = \int \sqrt{a\,k}\ dt$, while the final velocity reached is $v_f = \int a dt$. Thus, instability growth is worst for constant acceleration and can be substantially reduced by applying the acceleration in bursts. Even for constant acceleration, long wavelength growth ($\lambda \sim R$) is not severe, since, for $a \sim R/t^2$ and $k \sim R^{-1}$, $N \approx 1$.

Equation (6) shows that γ is largest for small wavelength perturbations. Very short wavelengths will be damped by viscous effects, but there exists a substantial wavelength range ($\lambda << \Delta R$) in which perturbations will grow rapidly to a nonlinear state. The resulting turbulent situation is expected to alter heat and momentum transport coefficients, but no adequate theory has been developed.

IV. Interpretation of Experiments

The laser-fusion implosion concept involves many complex phenomena.

Theoretical models predict that a laser fusion power plant is feasible, but the uncertainties are large. Experiments and the theoretical work involved in their interpretation will help to resolve these questions (and formulate new ones).

To date, theoretical models have been consistent with experiments. However, uncertainties in experimental configurations are also quite large. In some cases, several different models have been able to predict the same experimental observation, but such situations should become more infrequent as laser and plasma diagnostics improve. An historical example will serve to illustrate the dangers of incomplete diagnostics and oversimplified theoretical models.

In 1970 neutrons were detected from a deuterium ice slab irradiated by a neodymium laser[30]. One-dimensional hydrodynamic computer models calculated the correct number ($\sim 10^4$) of neutrons. The simplicity of the model and agreement with experiment were encouraging. However, when two-dimensional hydrodynamic calculations were performed, it was learned that sideways expansion of the plasma plume cooled the plasma substantially, resulting in a neutron yield of $< 10^2$. Several mechanisms (magnetic fields, laser light self-focusing, and direct ion heating by plasma instabilities) seemed to explain the "anomalous" neutrons. The neutrons turned out to be non-thermonuclear. They were produced by deuterons in the plasma blow-off colliding with either background gas[31], or the remains of previous experiments stuck on the target chamber wall[32].

A. Magnetic Fields

Magnetic fields are produced in all laser plasma experiments. We may estimate the field strength by extending Eq. (4) to include adiabatic field expansion

$$\dot{\underline{B}} = \underline{\nabla} \times [\underline{v} \times \underline{B} + \frac{c}{e n_e} \underline{\nabla} P_e] \qquad (7)$$

and by assuming steady state ($\dot{\underline{B}} = 0$). Ignoring the directions of the various vectors in this equation we obtain

$$B = \frac{ck\, T_e}{e\, H\, v}$$

where H is the temperature scale height (measured perpendicular to the density gradient) and $v \approx c_s$ is a characteristic matter velocity. Since $c_s \propto T_e^{1/2}$ the field strength depends only weakly on temperature.

$$B\ (MG) = 1.6\, T_e^{1/2}\ (H/20\,\mu m)^{-1} . \qquad (8)$$

The scale height H is difficult to estimate. If it is taken as the laser beam spot radius, then megagauss fields are expected. If, however, a spherical target was illuminated with good uniformity, H would be large and smaller fields would result. Filamentation of the plasma by light self-focusing might create scale heights comparable to the laser wavelength, leading to 10 MG fields for Nd light. In this case, however, electron conduction would rapidly smooth the temperature gradient. The situation begins to get complicated when we remember that the electron conductivity

depends (in an uncertain fashion) on B. Despite these difficulties, numerous two-dimensional MHD codes[18, 33-35] have calculated field strengths in agreement with magnetic probe measurements[20].

B. X-Ray Spectra from Slab Targets

McCall[36] has obtained high energy x-ray spectra from targets irradiated by both CO_2 and Nd lasers. Both targets were thick CH_2 plastic foils.

The CO_2 experiment used a 1.5 ns, 100 μm diameter laser beam. Figure 5a shows the high energy x-ray brightness for a 10 J (circles) and a 2 J (crosses) pulse. The theoretical curves[37] shown were calculated by the LASNEX[33] two-dimensional hydrodynamic-transport code. In this computer model the fraction of the incident laser energy that is absorbed by parametric instabilities and resonance absorption heats electrons by promoting them into a suprathermal energy distribution according to

$$\dot{n}(v) \quad \alpha\, v^2 \exp\left[-1/2\, m_e\, v^2 / \alpha k\, T_e\right] \tag{9}$$

where v is the velocity coordinate of the distribution (assumed isotropic) and $\alpha (6 \leq \alpha \leq 12)$ is an input parameter characterizing the heated distribution. At the time these calculations were performed α was believed to be about twelve[38]. (Subsequent plasma simulations[8] which account for a self-consistent density profile have found $\alpha = 6$ is

more correct.) Figure 5a shows that the agreement between this model and experiment is good at both laser energies. A calculation for the 10 J experiment using only inverse bremsstrahlung heating lacks the high-energy electron tail and thus produces very few x-rays with $h\nu > 10$ keV.

McCall's Nd laser experiment used a 10 J, 30 ps, 50 μm diameter beam. Figure 5b gives the experimental x-ray brightness and the results of LASNEX calculations for (1) 10 J absorbed and $\alpha = 12$, (2) 1 J absorbed and $\alpha = 12$, and (3) 10 J absorbed and an inverse bremsstrahlung electron distribution. The experimental spot diameter has subsequently been revised from 50 to 100 μm, (see Ref. 17) reducing the light intensity by a factor of four. This, together with the use of $\alpha = 6$ rather than $\alpha = 12$, helps to bring theory and experiment into agreement, but the calculation is still high. It is interesting that a completely different theoretical model[17] (using a reduced electron conductivity to produce very hot electrons in the low-density plasma plume) also requires a substantial reduction in absorbed energy in order to obtain agreement with this experiment. The reason for this is that the thermal x-ray emission ($\lesssim 15$ keV) is determined primarily by absorbed energy and is not very model dependent. The poor agreement with this experiment has not yet been resolved.

Figure 6 shows results of similar experiments[39] performed with the Livermore Janus (Nd, 10 J, 100 ps, 30 and 100 μm dia.) laser. The LASNEX

calculations[40] using $\alpha = 6$ show good agreement. The absorption parameters used to calculate these CH foil experiments are identical to those used in calculating the quite different experiment to be discussed in the following section.

C. Glass Ball and Disc

The Janus laser was used to irradiate a 55 μm diameter, 1/2 μm thick, sperhical glass microballoon[41] containing DT gas at density 2×10^{-3} g/cc. The microballoon was mounted on a 1/2 μm thick, 140 μm average diameter glass disc. The laser pulse was an 18 J, 90 ps FWHM Gaussian. The ring (low intensity on axis) beam had a diameter of $\sim$ 60 μm at target position.

The LASNEX calculations of this experiment[42] are in good agreement with the measured x-rays, neutrons and compression. The calculations show that the glass microballoon is supersonically penetrated by electron and x-ray transport and therefore explodes while it is pushed inwards by ablation pressure. This type of implosion is less sensitive to Taylor instabilities than the purely ablative isentropic implosions needed for laser fusion CTR. Compressions of $\sim 10^2$ were obtained but the peak density (<1g/cc) was much less than desired for fusion applications ($\geq 10^3$ g/cc). For the Janus laser pulse, however, an exploding pusher implosion produces higher ion temperatures and thus, higher neutron yields.

Calculations showed that the position of the compression peak (relative to the initial center of the microballoon) was very sensitive to the laser beam spatial profile. The beam was known to be ring-shaped and some amount of beam breakup (further reducing the on axis intensity) was expected. In the calculations, the beam profile was varied within experimental uncertainties to obtain agreement with the observed x-ray microscope picture. All other code inputs were experimentally known quantities or were obtained from theory. The parameters used to simulate parametric instabilities and resonance absorption ($\alpha = 6$, 25% absorbed when a laser ray reached 90% of critical density) were obtained from plasma simulation calculations and have consistently given good results for other types of experiments performed at LLL.

Comparison between the computer model and experiment is shown in Figure 7 (x-ray spectrum) and Figure 8 (on axis densitometer trace of x-ray emission). The calculated neutron yield ($\sim 10^4$) is in agreement. Because of the numerous uncertainties, however, the fraction of neutrons produced by thermonuclear (as opposed to beam-plasma) reactions cannot be inferred. This must wait for an experimental measurement of the DT ion temperature.

V. Conclusions

A laser-fusion power plant in which small DT droplets or shells are imploded to super-high densities appears to be theoretically feasible.

The extensive computer simulations used to analyze such systems, however, involve several physical uncertainties which have yet to be resolved experimentally. The basic laser fusion scheme has already been modified because of theoretical work and the results of future experiments will necessitate further modifications.

Because of preheat and decoupling effects, short wavelength lasers ($\lesssim 1/2$ m) may be needed to supply most of the energy near the end of the laser pulse. The high power requirements on the laser may be reduced by using shell targets; but in this case $R/\Delta R \leq 5$ must be maintained in order to minimize shell breakup due to fluid instabilities. Applying the laser energy in bursts can help to reduce such instabilities by producing an impulsive (but nearly isentropic) implosion. During the initial phases of the implosion long wavelength ($\gtrsim 4\,\mu$m) light may be necessary to obtain good symmetry. Illumination uniformity to 10% and normality to within 30° are probably needed.

In almost all cases, theory and experiment are in good agreement, but uncertainties are large in each.

REFERENCES

1. J. Nuckolls, L. Wood, R. Thiessen, and G. Zimmerman, Nature 239, 139 (1972).

2. J. S. Clarke, H. N. Fischer, and R. J. Mason, Phys. Rev. Letters 30, 89 (1973).

3. K. A. Brueckner, Trans. IEEE PS1, 13 (1973).

4. To obtain this formula, start with a uniformly-heated sphere, run a rarification wave inward from the surface at speed c_s, and assume that no reactions occur outside the rarification wave.

5. R. E. Kidder, Nucl. Fusion 14, 797 (1974).

6. J. D. Lindl and W. C. Mead, Phys. Rev. Letters 34, 1273 (1975).

7. T. W. Johnston and J. M. Dawson, Phys. Fluids 16, 722 (1973).

8. K. G. Estabrook, E. J. Valeo, and W. L. Kruer, UCRL-75613 (1975), submitted to Phys. Fluids.

9. E. J. Valeo and K. G. Estabrook, Phys. Rev. Letters 34, 1008 (1975).

10. D. Forslund, J. Kindel, and E. Lindman, Phys. Rev. Letters 30, 739 (1973).

11. W. L. Kruer, K. G. Estabrook, and K. H. Sinz, Nucl. Fusion 13, 952 (1973).

12. W. L. Kruer, E. J. Valeo, and K. G. Estabrook, UCRL-76612, (1975).

13. M. Lubin, E. Goldman, J. Sources, L. Goldman, W. Friedman, S. Letzring, J. Albritton, P. Koch, and B. Yaakobi, in Plasma Physics and Controlled Nuclear Fusion (IAEA, Vienna, Austria, 1974).

14. K. Mizuno and J. S. DeGroot, University of California, Davis R-4 (1975), submitted to Phys. Rev. Letters.

15. L. Spitzer, Physics of Fully Ionized Gases, 144 (Interscience Publishers, New York, 1962).

16. B. D. Fried and R. W. Gould, Phys. Fluids, 4, 139 (1961).

17. R. C. Malone, R. L. McCrory, and R. L. Morse, Phys. Rev. Letters 34, 721 (1975).

18. J. B. Chase, J. M. LeBlanc, and J. R. Wilson, Phys. Fluids 16, 1142 (1973).

19. J. J. Thomson, C. E. Max, and K. G. Estabrook, UCRL-76690 (1975), submitted to Phys. Rev. Letters.

20. J. A. Stamper, K. Papadopoulous, S. O. Dean, E. A. McClean, and J. M. Dawson, Phys. Rev. Letters 26, 1012 (1972).

21. J. A. Stamper and B. H. Ripin, Phys. Rev. Letters 34, 138 (1975).

22. S. I. Braginskii, in Reviews of Plasma Physics, (Consultants Bureau, New York, 1965), vol. 1, p. 205.

23. L. Spitzer, Phys. Fluids 3, 659 (1960).

24. D. Bohm, in Characteristics of Electrical Discharges in Magnetic Fields, (McGraw-Hill, New York, 1949), Chapter 2, Sec. 5.

25. R. E. Kidder and J. Zink, Nucl. Fusion 12, 325 (1972).

26. J. D. Lindl, Nucl. Fusion 14, 511 (1974).

27. J. N. Shiau, E. B. Goldman, and C. I. Weng, Phys. Rev. Letters 32, 352 (1974).

28. D. B. Henderson, R. L. McCrory, and R. L. Morse, Phys. Rev. Letters 33, 205 (1974).

29. G. Taylor, Proc. Royal Society 201, A, 192 (1950).

30. F. Floux, D. Cognard, L. Denoeud, G. Piar, D. Parisot, J. Bobin, F. Delobeau, and C. Fauquignon, Phys. Rev. A1, 821 (1970).

31. J. I. Katz, Appl. Phys. Letters 23, 342 (1973).

32. G. H. McCall, F. Young, A. W. Ehler, J. F. Kephart, and R. P. Goodwin, Phys. Rev. Letters 30, 1116 (1973).

33. G. B. Zimmerman, UCRL-74811 (1973).

34. M. Widner and T. Wright, Sandia Laboratories SC-DR-720733 (1973).

35. D. Colombant, K. Whitney, N. K. Winsor, J. Davis, and D. A. Tidman in Naval Research Laboratory Report 7838 (1974), p. 135.

36. J. F. Kephart, R. P. Godwin and G. H. McCall, Appl. Phys. Letters 25, 108 (1974).

37. J. H. Nuckolls, G. H. Dahlbacka, J. D. Lindl, W. C. Mead, H. D. Shay, A. R. Thiessen, and G. B. Zimmerman, in UCRL-50021-73-2 (1973), p. 72.

38. J. I. Katz, J. Weinstock, W. Kruer, J. DeGroot, and R. Faehl, Phys. Fluids 16, 1519 (1973).

39. E. Storm and H. Kornblum, private communication (1975).

40. W. C. Mead, private communication (1975).

41. J. Holzrichter, H. Ahlstrom, R. Speck, E. Storm, J. Swain, L. Coleman, C. Hendricks, H. Kornblum, F. Seward, V. Slivinsky, Y. Pan, G. Zimmerman, and J. Nuckolls, UCRL-76860 (1975), submitted to Phys. Rev. Letters.

42. Y. L. Pan, G. B. Zimmerman, and J. H. Nuckolls, UCRL-76865 (1975), submitted to Phys. Rev. Letters.

FIGURE CAPTIONS

Figure 1 Calculated gain (TN energy/laser energy) versus compression for different laser energies.

Figure 2 Near optimal pulse shape for a 5×10^4 J laser irradiating a 50 μg liquid DT drop.

Figure 3 Fractional absorption by parametric instabilities and resonance absorption versus angle of incidence. The light intensity is 10^{16} W/cm^2 and the density profile has relaxed to equilibrium.

Figure 4 Heated electron distribution in arbitrary units versus electron momentum for (a) parametric instabilities and (b) resonance absorption. Dotted curve is the initial distribution.

Figure 5 X-ray spectra from LASL experiments on CH_2 foils.

(a) CO_2, 10 J (circles) and 2 J (crosses), 1.5 ns, 100 μm dia. Result from LASNEX calculations for 10 and 2 J ($\alpha = 12$) and with inverse bremsstrahlung only.

(b) Nd, 10 J, 30 ps, 50μm dia. Results from LASNEX calculations for 10 and 1 J ($\alpha = 12$) and with thermal radiation only.

Figure 6 X-ray spectra from LLL experiment on CH discs. (Nd, 10 J, 100 ps) and results of corresponding LASNEX calculations.
(a) 30 m dia. spot
(b) 75 m dia. spot.

Figure 7 X-ray spectrum from LLL ball and disc experiment (open circles). (Nd, 18 J, 90 ps, 60 m dia.) and results of LASNEX calculation (filled circles).

Figure 8 Calculated and measured densitometer traces along symmetry axis from x-ray microscope pictures of ball and disc experiment.

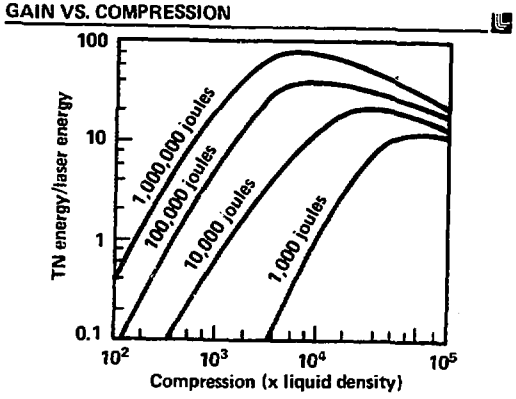
GAIN VS. COMPRESSION
100
10
1
0.1
TN energy/laser energy
1,000,000 joules
100,000 joules
10,000 joules
1,000 joules
10^2
10^3
10^4
10^5
Compression (x liquid density)

FIGURE 1

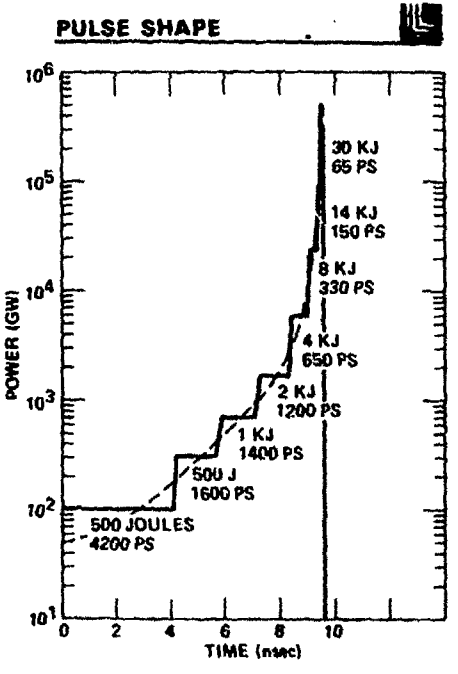
PULSE SHAPE
POWER (GW)
10^6
10^5
10^4
10^3
10^2
10^1
30 KJ
65 PS
14 KJ
150 PS
8 KJ
330 PS
4 KJ
650 PS
2 KJ
1200 PS
1 KJ
1400 PS
500 J
1600 PS
500 JOULES
4200 PS
0
2
4
6
8
10
TIME (nsec)

FIGURE 2

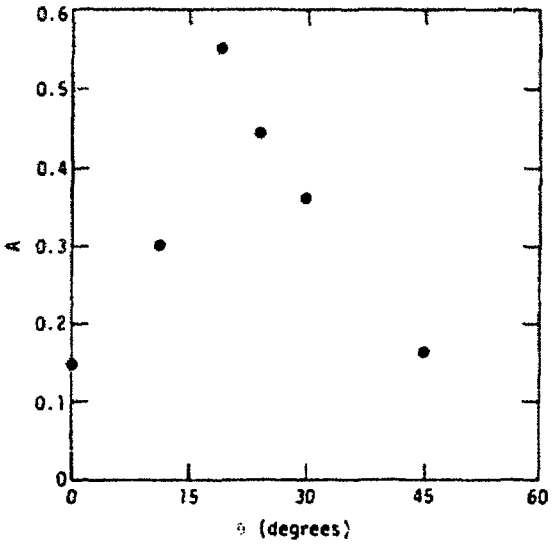

FIGURE 3

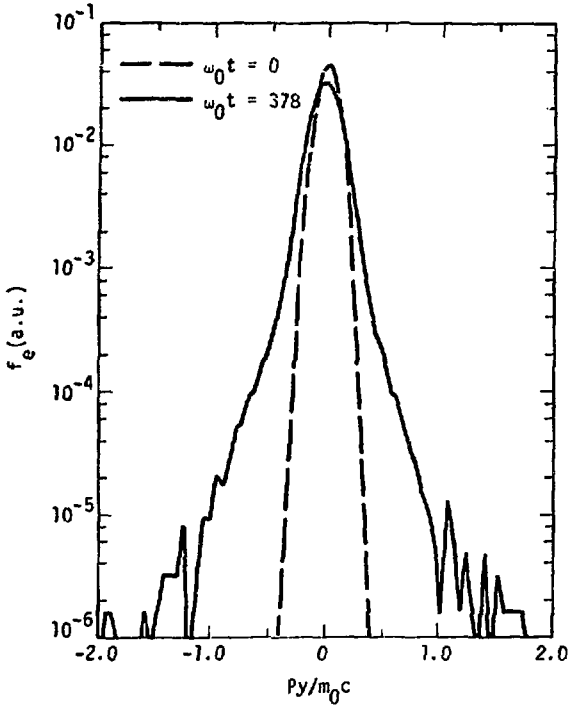
10^{-1}
10^{-2}
10^{-3}
10^{-4}
10^{-5}
10^{-6}
f_e(a.u.)
$\omega_0 t$ = 0
$\omega_0 t$ = 378
-2.0
-1.0
0
1.0
2.0
Py/m_0c

FIGURE 4(a)

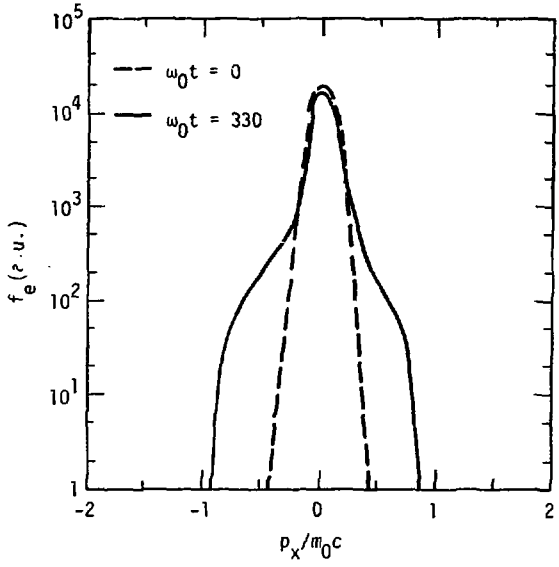

FIGURE 4(b)

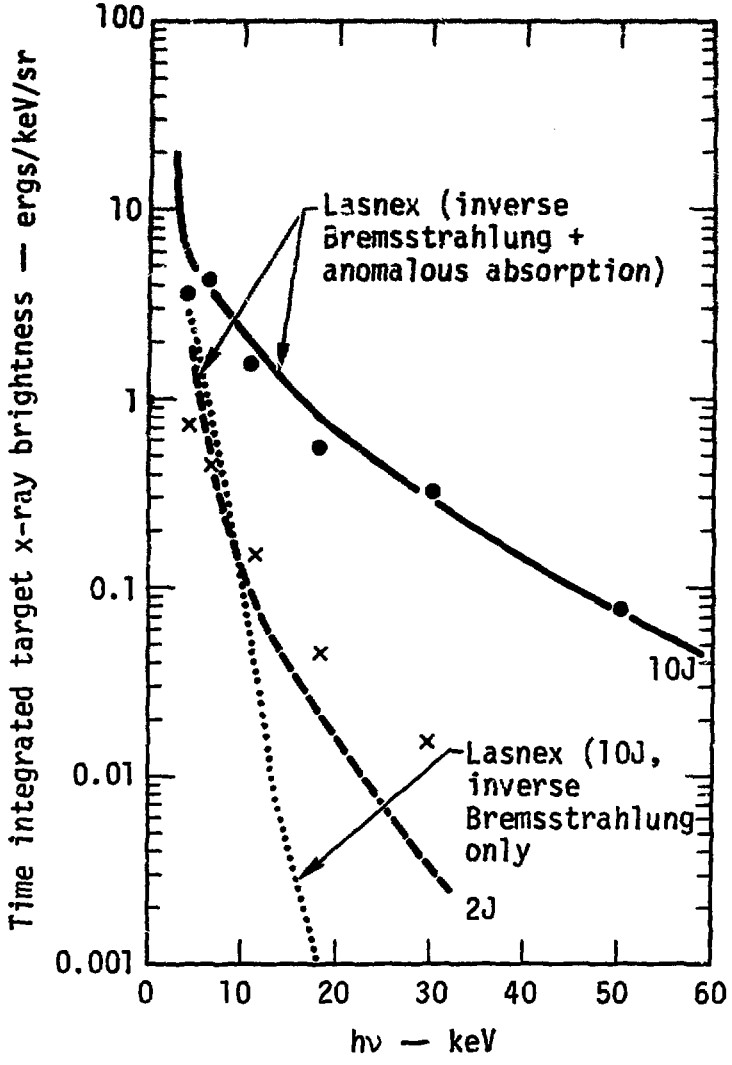
100
10
1
0.1
0.01
0.001
0
10
20
30
40
50
60
Time integrated target x-ray brightness — ergs/keV/sr
hν — keV
Lasnex (inverse Bremsstrahlung + anomalous absorption)
10J
Lasnex (10J, inverse Bremsstrahlung only
2J

FIGURE 5(a)

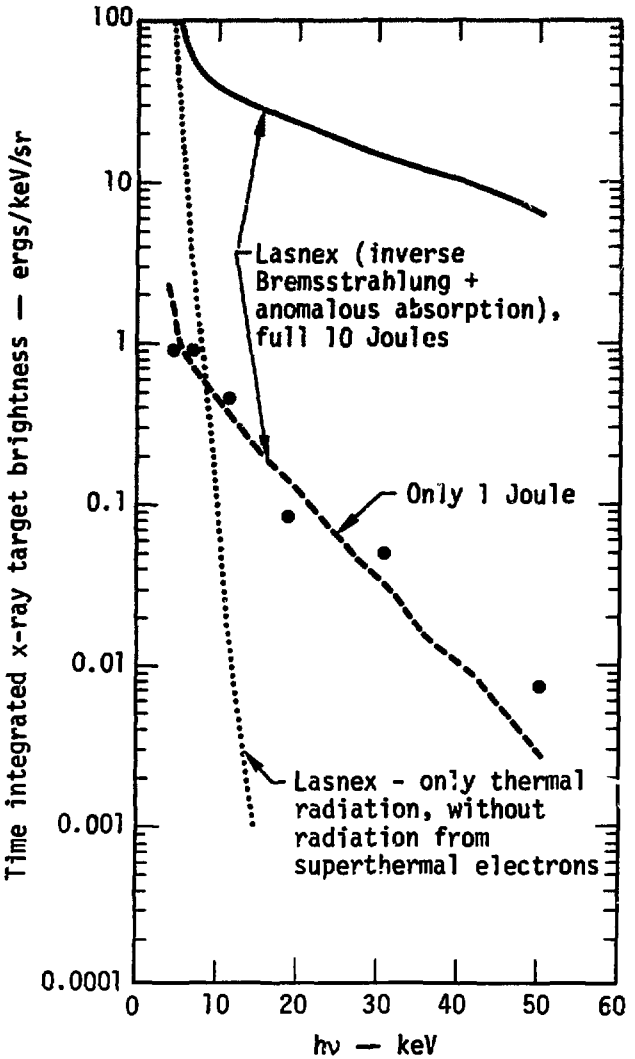
Time integrated x-ray target brightness — ergs/keV/sr
100
10
1
0.1
0.01
0.001
0.0001
0
10
20
30
40
50
60
hν — keV
Lasnex (inverse Bremsstrahlung + anomalous absorption), full 10 Joules
Only 1 Joule
Lasnex - only thermal radiation, without radiation from superthermal electrons

FIGURE 5(b)

X-RAY INTENSITY VS ENERGY FOR PARYLENE DISK
1.06 μm LASER, 11 J, 100 ps FWHM, 30 μm SPOT DIAMETER

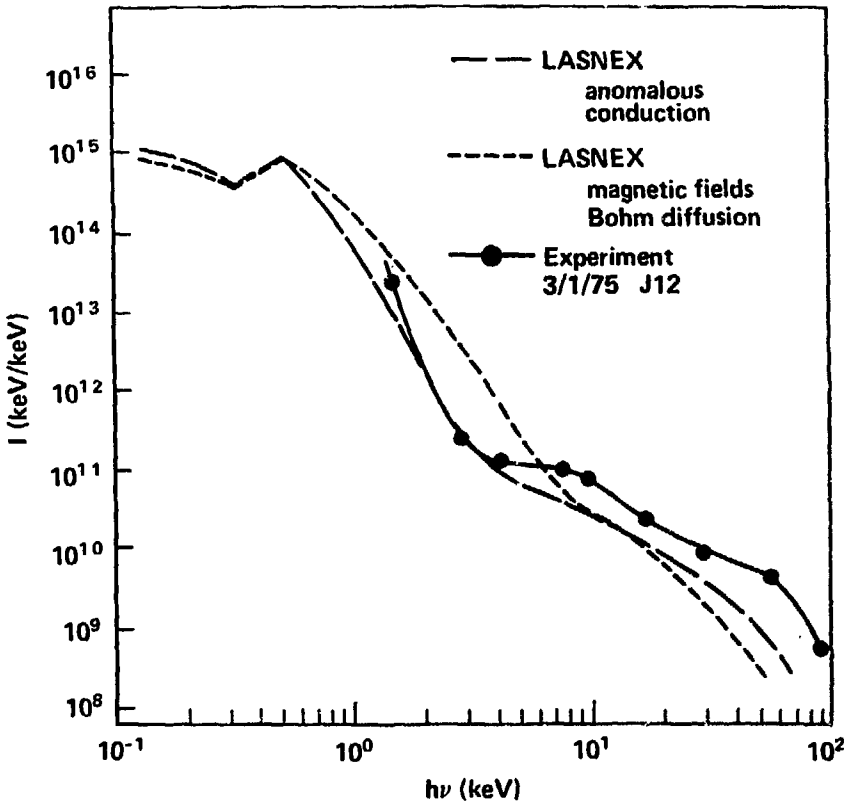

FIGURE 6(a)

X-RAY INTENSITY VS ENERGY FOR PARYLENE DISK
1.06 μm LASER, 8 J, 100 ps FWHM, 75 μm SPOT DIAMETER

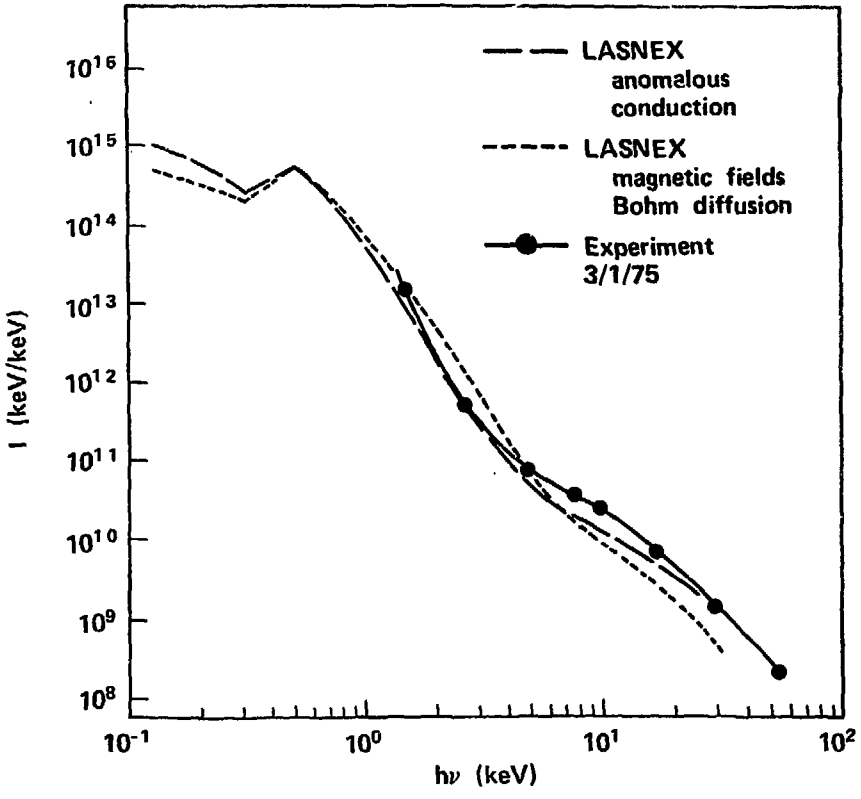

FIGURE 6(b)

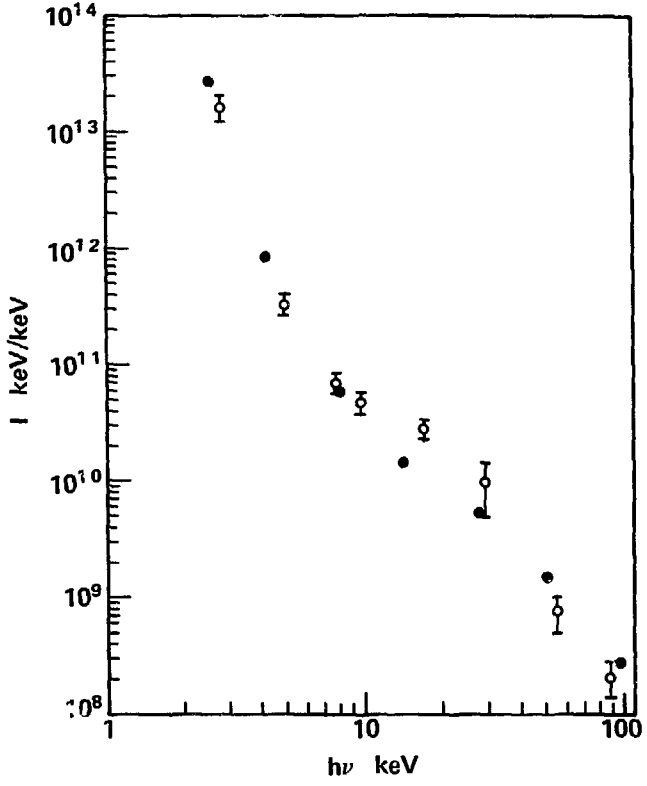

FIGURE 7

DENSITOMETER TRACE ALONG SYMMETRY AXIS

FIGURE 8

Printed in the United States of America
Available from
National Technical Information Service
U. S. Department of Commerce
5285 Port Royal Road
Springfield, Virginia 22151
Price: Printed Copy $___*; Microfiche $2.25

*Pages	NTIS Selling Price
1-50	$4.00
51-150	$5.45
151-325	$7.60
326-500	$10.60
501-1000	$13.60